2009

Controlled synthesis of core/shell magnetic iron oxide/carbon systems via a self-template method

Shenmin Zhu
Shanghai Jiao Tong University

Di Zhang
Shanghai Jiao Tong University

Z. Chen
University of Wollongong, zchen@uow.edu.au

Yimu Zhang
Shanghai Jiao Tong University

Controlled synthesis of core/shell magnetic iron oxide/carbon systems *via* a self-template method†

Shenmin Zhu,*[a] Di Zhang,*[a] Zhixin Chen[b] and Yimu Zhang[a]

Received 18th June 2009, Accepted 13th August 2009
First published as an Advance Article on the web 2nd September 2009
DOI: 10.1039/b912057b

A sol-gel assembly process was developed for the synthesis of magnetic core/carbon shell materials with porous networks. $Fe(CO)_5$ was assembled into the pore channels of mesoporous silica *via* a sol-gel method at 18 °C, by using the block copolymer F127 as the template and $Fe(CO)_5$ as an additional precursor. At this temperature, the magnetic precursor $Fe(CO)_5$ was pre-organized into hydrophobic cores of micelles by self-assembly of F127. In the subsequent carbonization of the assembly under an Ar atmosphere, $Fe(CO)_5$ transformed into magnetic nanoparticles and surfactant F127 transferred into carbon shells enveloping the magnetic nanoparticles, forming magnetic iron oxide core/carbon shell structures. The removal of the silica with 5% HF acid resulted in the core/shell nanoporous composite. The obtained system demonstrates a saturation magnetic value of 3 emu g^{-1} as well as a high surface area (98 cm^2 g^{-1}) and pore volume (0.21 m^3 g^{-1}), which would benefit its potential applications as adsorbents and catalysts, or applications in targeted drug delivery systems. This facile strategy would provide an efficient approach for tailoring core/shell porous materials with desired functionalities and structures by adjusting precursors and structure-directing agents.

Introduction

Hybrid core/shell magnetic materials are creating great interest in biotechnology.[1] The hybrid nature provides a high chemical specificity,[2,3] which has been used to tailor materials with desirable functionalities. As they can be manipulated by an external magnetic-field gradient, the core/shell magnetic materials have great potential for use as contrast agents for magnetic resonance imaging,[3–8] used in magnetic separations of bacteria/protein from biotemplates,[9] and in targeted drug deliveries.[10]

For technological applications, such as enzyme immobilization, drug delivery and separations of molecules in complex systems, the magnetic materials are needed to be nontoxic, stable and as fine as possible. The magnetic materials must also have a reversible magnetic behavior to inhibit aggregation effects. A widely accessible and adjustable porous network will further improve the functionality of the nano magnetic materials. Iron oxides, ferrites, magnetite and/or maghemite, are by far the most commonly employed in biotechnology because they are stable and nontoxic and have an adequate magnetic moment.[11,12] Several attempts to synthesize materials with these characteristics have been reported. Unfortunately, most of the methods produced either nonporous magnetic composites,[13–15] or porous composites in which the magnetic materials are not homogeneously distributed,[16] or porous materials frequently displaying magnetic memory.[17,18]

In the past few decades, much effort has focused on the fabrication of mesoporous carbon (MC) because of its unique properties, including highly ordered structures, large surface area, and narrow distribution of pore sizes.[19] Despite considerable progress in the synthesis of MC, there is still no reliable processes of introducing magnetism into MC while retaining their porous systems.[20] The commonly employed strategy to synthesize magnetic carbon materials is the condensation of divalent or trivalent iron salts in carbon in the presence of hydroxide with a subsequent calcination.[21] Such a synthetic procedure, however, generally leads to a substantial blocking of pore spaces. In 2004, Schuth *et al.* described an approach towards the fabrication of an ordered mesoporous carbon with surface grafted magnetic particles, by a combination of nanocasting and spatially selective deposition.[22] The protection of magnetic nanoparticles was achieved by a carbon layer. Although this technology is promising, it often involves a fairly long and complicated process. Recently, Li *et al.* described a simplified route for the fabrication of hybrid core/shell materials based on Pt nanoparticles inside mesoporous carbon channels.[23] The nanohybrid structures were realized through two steps: first, a hydrothermal process was employed to infiltrate and deposit Pt nanoparticles inside SBA-15, and second, the formation of carbonaceous products by polymerization of the SBA-15 through the use of glucose as the reductant as well as the carbon source. Clearly, the use of hard templates is still unavoidable. With this post synthesis process, the efficiency of the deposition of Pt was controlled by the diffusion of Pt. How to synthesize core/shell materials in a controlled facile method is still the biggest challenge.

Here, we report for the first time a sol-gel assembly process for the fabrication of a core/shell magnetic iron oxide/carbon porous composite, with uniformly distributed magnetic nanoparticles.

[a]*State Key Lab of Metal Matrix Composites, Shanghai Jiao Tong University, 200240 Shanghai, P. R. China. E-mail: smzhu@sjtu.edu.cn; zhangdi@sjtu.edu.cn; Fax: +86-21-34202749; Tel: +86-21-34202584*
[b]*The Faculty of Engineering, University of Wollongong, Wollongong, NSW 2522, Australia*

† Electronic supplementary information (ESI) available: Supplementary figures. See DOI: 10.1039/b912057b

These composites show no magnetic memory and the structures of the composites can be easily manipulated in a sol-gel process.

Inspired by the phenomenon that hydrophobic functionality of 1,3,5-trimethylbenzene (TMB), which is a swelling agent, can be used in the preparation of mesoporous materials, we chose hydrophobic $Fe(CO)_5$ as the magnetic precursor source, and a simple method of the self-assembly of core/shell magnetic iron oxide/carbon porous materials (MI@CP) was pioneered. One of the applications of this MI@CP as a magnetically separable adsorbent is demonstrated in this study.

Experimental

Synthesis of the materials

Triblock poly(ethylene oxide)-*b*-poly(propylene oxide)-*b*-poly(ethylene oxide) copolymer $EO_{106}PO_{70}EO_{106}$ (Pluronic P127, $M_w = 13400$) was purchased from Aldrich. All chemicals were used as received without purification. In a typical synthesis, 1.5 g of F127 and 7.5 g of KCl, were dissolved in 90 ml of HCl (2 M). After 2 h stirring, 2 ml $Fe(CO)_5$ was poured into the solution and stirred for a further 2 h at a fixed temperature ($T = 16$–$18, 45$ °C). Then, 6.24 g of TEOS was added to this solution, and stirred for 24 h at the same temperature. The molar ratio of the reactants is $F127 : TEOS : Fe(CO)_5 : KCl : HCl : H_2O = 3.7 \times 10^{-3} : 1 : 0.74 : 3.3 : 6 : 167$. The solution along with the precipitate was then removed to an autoclave and hydrothermally treated by putting in an oven for another 24 h at 80 °C. The product was filtered and washed several times with distilled water and dried at 60 °C. The calcination was performed at 520 °C under Ar, the obtained sample is denoted as MI@CP/SBA-16. The final product was obtained by the removal of the silica using 5% HF for 12 h.

Adsorption of methylene blue

The adsorption of methylene blue (MB) on core/shell MI@CP was conducted as below: 10 mg of core/shell MI@CP and 30 ml MB stock solutions of different concentration were mixed and shaked in distilled water at 25 °C. The mixture was filtered and the residual MB concentration in the filtrate was measured using a spectrophotometer at a wavelength of 662 nm.

Structural characterization

The synthesized samples were characterized by X-ray diffraction (XRD) using a RigakuD/max2550VL/PC system operated at 1600-W power (40 kV, 40 mA) with Cu KR radiation (λ 1.5406 Å), at a scan speed of 5° min^{-1} and a step size of 0.050° in 2θ. Nitrogen adsorption measurements at 77 K were performed using an ASAP2020 volumetric adsorption analyzer, after the samples had been outgassed for 8 h in the degas port of the adsorption apparatus. Transmission electron microscope (TEM) and energy-dispersive X-ray (EDX) measurements were carried out on a JEOL 2010 microscope. TEM specimens were prepared by grinding the synthesized samples into powder with a mortar and pestle and the powder was dispersed in pure ethanol and picked up with holey carbon supporting films on copper grids.

Results and discussion

The process is schematically described in Fig. 1. Firstly, mesostructured silica SBA-16 with magnetic precursors $Fe(CO)_5$ inside, denoted as $Fe(CO)_5$/SBA-16, was assembled *via* a surfactant template route. Secondly, magnetic iron oxide nanoparticles formed *in situ* during the thermal treatment at 520 °C in argon, which were surrounded by a layer of carbon resulted from the carbonization of the surfactant F127 at the same temperature (the sample is denoted as MI@CP/SBA-16). Finally, the silica was dissolved by using 5% HF and the core/shell MI@CP composite was obtained. During the synthesis process, the assembly temperature was set at 18 °C with a molar ratio of $Fe(CO)_5$ to TEOS of 0.74.

The composites were firstly examined by small-angle X-ray diffraction (SXRD) as shown in Fig. 2a. The as-synthesized $Fe(CO)_5$/SBA-16 shows a well-resolved diffraction peak at $2\theta \approx 0.65°$. Compared with the pure SBA-16 ($2\theta \approx 1.00°$), the distinct shift of the diffraction peak to the lower angle was attributed to the introduction of $Fe(CO)_5$ inside the pores, suggesting the swelling of the micelles in the presence of $Fe(CO)_5$. After the heat-treatment in Ar gas atmosphere, the diffraction peak shifted to a higher angle, *i.e.*, $2\theta \approx 0.93°$ for MI@CP/SBA-16, due to the structural shrinkage resulting from the carbonization. Similar to the pure cubic SBA-16 prepared without the presence of $Fe(CO)_5$, the pattern of the calcined material (MI@CP/SBA-16, Fig. 2a) shows two well-resolved peaks with *d*-spacings of 9.5 and 6.9 nm, which can be indexed as (110), and (200) of the body-centered cubic structure (bcc, space group *Im3m*), with a lattice parameter of 13.5 nm. In contrast, the as-prepared mesostructured $Fe(CO)_5$/SBA-16 shows only one distinct diffraction peak and the (200) diffraction peak is hardly discernible. The disappearance of the (200) peak is probably due to the fact that the

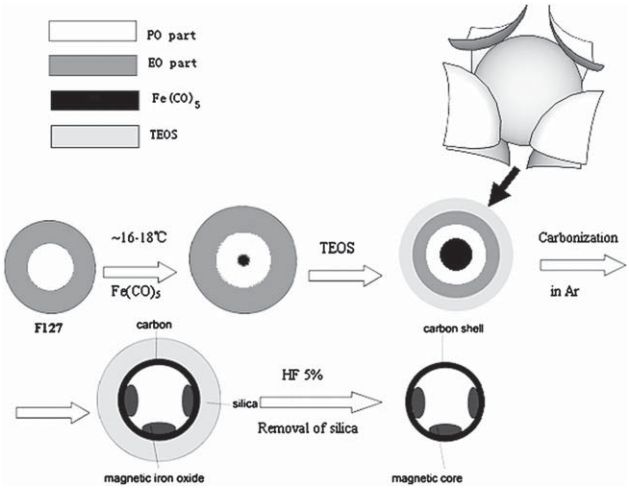

Fig. 1 A schematic illustration of the synthetic procedure of the core/shell magnetic iron oxide/carbon with porous network *via* a sol-gel method: (1) $Fe(CO)_5$ penetration into the hydrophobic core of the micelles formed by F127 at a low temperature; (2) assembly of mesostructured silica of cubic phase in the solution, forming $Fe(CO)_5$/SBA-16; (3) carbonization under Ar atmosphere to transfer $Fe(CO)_5$ into magnetic iron oxide and F127 into the carbon layer enveloping the magnetic cores as shell (MI@CP/SBA-16); (4) removal of silica by using 5% HF to yield core/shell MI@CP porous composites.

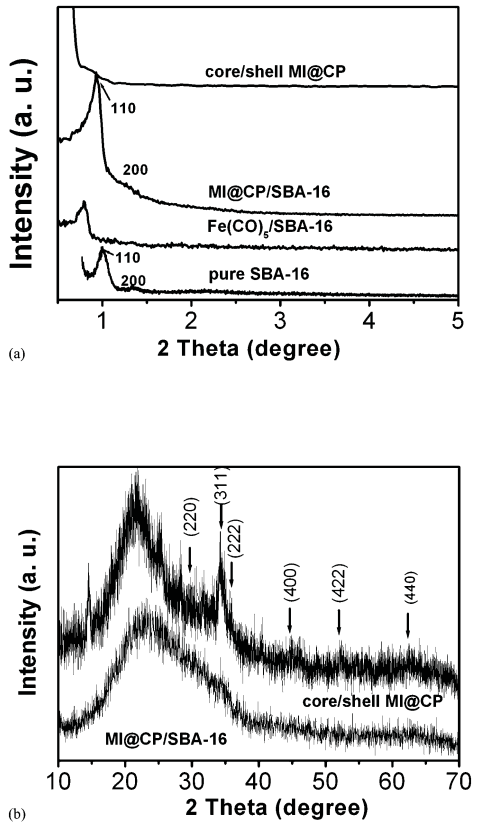

Fig. 2 (a) Small angle XRD patterns of the as-synthesized $Fe(CO)_5$/SBA-16, the calcined sample MI@CP/SBA-16, the sample after removal of silica by using 5% HF to obtain core/shell MI@CP materials, and with pure SBA-16 as a comparison prepared under the same conditions without the presence of $Fe(CO)_5$ calcined under an Ar atmosphere. (b) Wide angle XRD patterns of the samples MI@CP/SBA-16 before removal of silica and the final core/shell MI@CP.

(200) peak itself is very weak and that the pores of the SBA-16 were largely filled with $Fe(CO)_5$ precursor. After the removal of the silica from the MI@CP/SBA-16 using 5% HF, the resultant core/shell MI@CP composite displays a broad peak at $2\theta \approx 0.7$–$1.3°$, indicating that the ordered porous structure was damaged,[24,25] which is consistent with the TEM results shown later.

Fig. 2b shows the wide-angle XRD patterns of the composites before and after the removal of the silica matrix, corresponding to MI@CP/SBA-16 and the core/shell MI@CP, respectively. No distinct diffraction peaks were observed for the sample MI@CP/SBA-16. After removal of silica, the core/shell MI@CP composite exhibits a broad peak at about 23°, corresponding to the carbonized carbon and six characteristic diffraction peaks of crystalline Fe_3O_4 or γ-Fe_2O_3.[26] The average size of the particles, calculated with the Scherrer equation from the reflection at about $2\theta \approx 34.5°$, is around 3–4 nm. The extremely small size of the iron oxides makes it very difficult to be certain if they were Fe_3O_4 or γ-Fe_2O_3. It is currently accepted that Fe_3O_4 or γ-Fe_2O_3 are very similar in terms of lattice parameter and magnetic properties and thereby it is difficult to distinguish between them.[27] A similar phenomenon has been reported by many others in the pyrolysis of $Fe(CO)_5$ under different atmospheres.[28]

The bcc mesostructure of the as-prepared $Fe(CO)_5$/SBA-16 is confirmed by transmission electron microscopy (TEM). The mesostructure arrangements with long-range order are visible along the [111] and [110] directions, corresponding to Fig. 3a and b, respectively.[29] Combined with the corresponding XRD patterns, the ordered cubic (*Im3m*) mesostructure is further confirmed from these images. The calcined MI@CP/SBA-16 has a similar mesostructure as well, which is analogous to a bcc system, indicating that the ordered mesostructure is thermally stable (Fig. 3c–d, taken along the [111] and [110] directions, respectively). After the removal of the silica from MI@CP/SBA-16, the obtained core/shell magnetic iron oxide nanoparticles inside carbon (core/shell MI@CP) had a morphology as displayed in Fig. 3e–f, indicating the formation of magnetic nanoparticles homogenously inside the pores. The size of the nanoparticles is around 2–4 nm (Fig. 3e–f), which is almost identical to the value estimated from XRD. Clearly, there is no obvious magnetic iron oxide aggregation during the

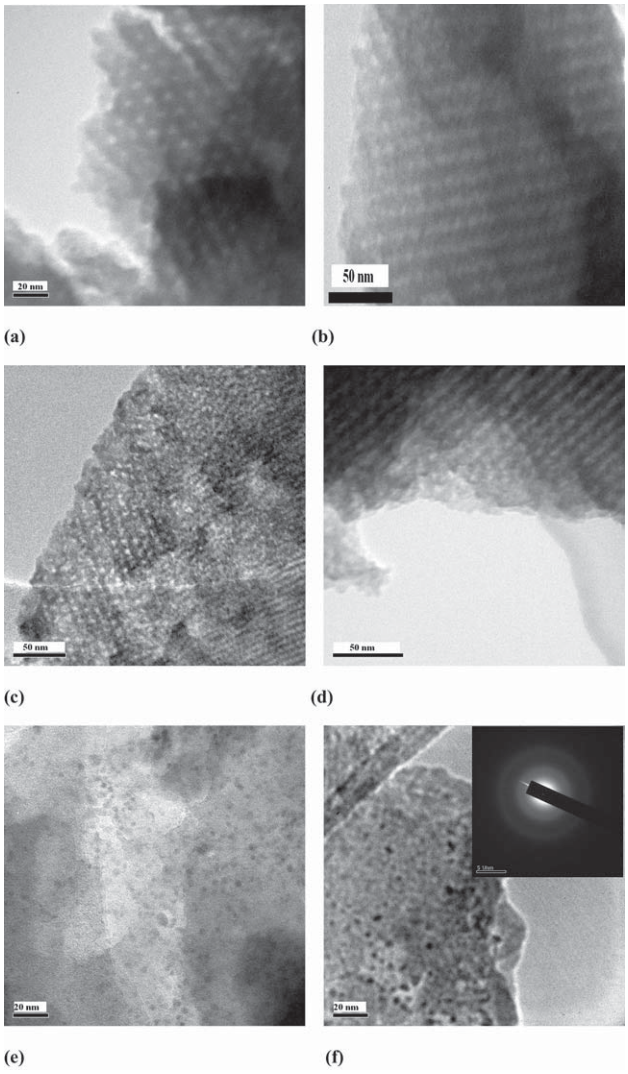

Fig. 3 TEM images of (a–b) as-prepared $Fe(CO)_6$/SBA-16 along [111] and [110] directions, (c–d) MI@CP/SBA-16 along the [111] and [110] directions, and (e, f) the core/shell MI@CP composite with a porous network.

carbonization and the removal of the SBA-16 silica. Fig. 3g shows the corresponding electron diffraction pattern of the core/shell MI@CP composites. The very diffused diffraction rings resulted from the low crystallinity as well as the extremely small size of the iron oxide particles. This result is consistent with the results of the XRD on the composite.

The core/shell structures of MI@CP were confirmed directly by high-resolution TEM (HRTEM) images shown in Fig. 4. It can be seen that the small individual nanocrystalline magnetic iron oxides (*ca.* 2–4 nm) are surrounded by many small and wrinkled lines, *i.e.* the magnetic nanoparticles are covered by a thin layer of carbon film which prevents the nanoparticles from agglomeration. Energy-dispersive X-ray spectroscopy (EDX) (Fig. 4c) results also confirm that the SBA-16 silica was almost completely removed by 5% HF. It is noteworthy that the iron oxide particles do not sinter even after thermal treatment at temperatures up to 520 °C. This can be attributed to the effect of passivation and stabilization of carbon layers on the iron oxide nanoparticles. The formation of the carbon layer was preferentially induced on iron particles because the carbonization of the copolymers is strongly catalyzed by iron.

Nitrogen absorption studies of the core/shell MI@CP show that the composite has a porous network of core/shell MI@CP as shown in Fig. 5. The isotherm curves are of type IV, and exhibit a hysteresis loop (H2) in the relative pressure range of 0.5–0.85 (P/P_0). The nitrogen adsorption/desorption measurements reveal that the core/shell MI@CP has a pore volume of 0.21 $cm^3\ g^{-1}$ and Brunauer–Emmett–Teller (BET) surface area of 98 $m^2\ g^{-1}$. The

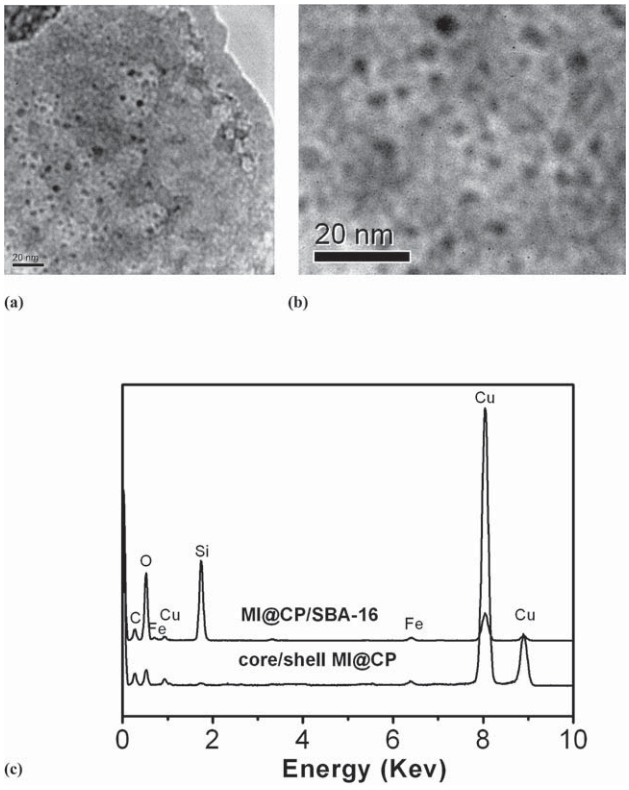

Fig. 4 HRTEM image of the core/shell MI@CP nanocomposite (a) at low magnification, (b) at high magnification. (c) EDX spectrum acquired for the resultant core/shell MI@CP sample.

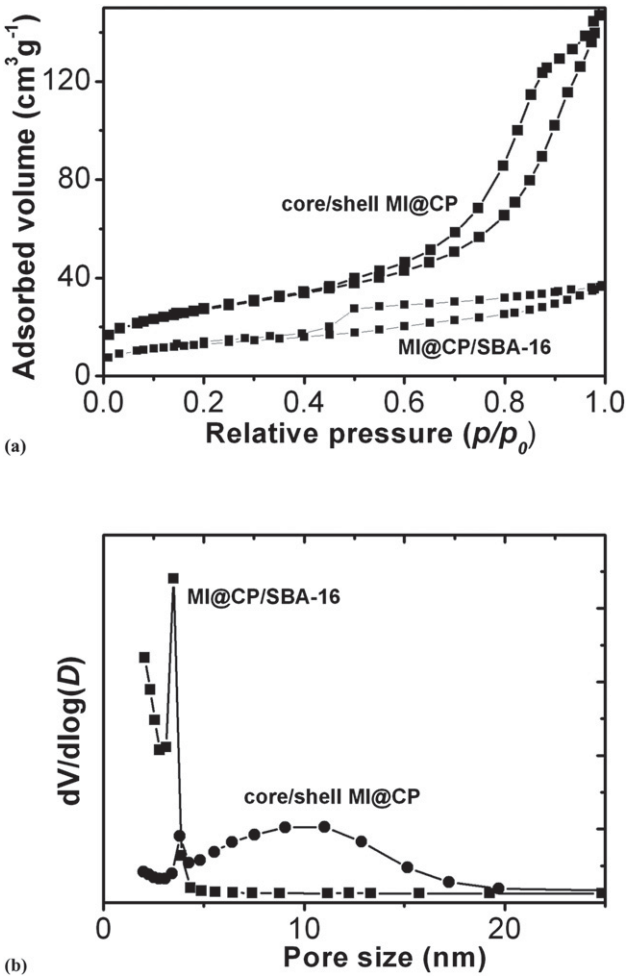

Fig. 5 (a) Nitrogen adsorption isotherms of the materials prepared at 18 °C. (b) The pore size distribution obtained by using the Barrett–Joyner–Halanda (BJH) model.

composite has pore size distributions in the mesoporous range and a very accessible pore system. As a comparison, the sample prepared under the same conditions as MI@CP except it was calcined in air has a much lower pore volume and BET surface area at 0.006 $cm^3\ g^{-1}$ and 2.1 $m^2\ g^{-1}$, respectively (see ESI†, Fig. S1), affording an additional evidence of porous carbon in the MI@CP composite which formed from the surfactant inside the pores of the as-synthesized $Fe(CO)_5$/SBA-16. The isotherm of the core/shell MI@CP composite possesses two hysteresis loops in the relative pressure range of 0.4–0.6 and 0.7–0.9, respectively. This indicates the existence of two pore size systems. The pore size distribution of the core/shell MI@CP composite, calculated from the adsorption branch of the isotherm using the BJH (Barrett–Joyner–Halenda) algorithm, exhibits a sharp peak at 3.8 nm accompanied by a broad peak at about 10.8 nm (Fig. 5b), *i.e.* the composites have a pore size distribution with a bimodal pore structure. Generally, the pore sizes of mesoporous carbon reported so far are roughly equal to the thickness of the respective parent silica pore walls (around 4 nm). Therefore, the smaller mesopores at around 3.8 nm could be the measurement of the inside diameter of the carbon cylinders or the mesopores created from the dissolution of the silica walls.

The larger pores with a mean diameter of 10.8 nm, can be the result of interconnections between adjacent channels where the carbon layers are partially missing, as described in the preparation of PAN-based OMC with bimodal pore size distributions.[30] The increase of the specific surface area to 98 $cm^2\ g^{-1}$ (core/shell MI@CP) from 47 $cm^2\ g^{-1}$ (MI@CP/SBA-16) and the change of the pore structure to a bimodal (core/shell MI@CP) from a unimodal (MI@CP/SBA-16) after the removal of silica, further confirmed the core/shell porous structures of the resultant MI@CP composites.

In our previous work, it was observed that hydrophobic $Fe(CO)_5$ may penetrate into the hydrophobic core of micelles formed by the triblock copolymer of $E_{20}PO_{70}EO_{20}$ (P123) at the assembled temperature of 45 °C.[31] However, a similar process could not be used to synthesize magnetic iron oxide inside SBA-16, because the large moiety of the hydrophilic chains in the block copolymer F127 ($EO_{106}PO_{70}EO_{106}$) may hinder the penetration of hydrophobic $Fe(CO)_5$ in the micelle cores at this temperature. This possibly explains why only a very small amount of iron oxide/C composites was obtained in a series of comparison experiments at relatively high temperatures (25–40 °C) (not shown here). Significantly, we observed a distinct crystallization of $Fe(CO)_5$ during the thermal-treatment process at 80 °C, due to the presence of a large amount of $Fe(CO)_5$ outside the micelle cores (see ESI†, Fig. S2). A similar phenomenon was also observed by Zhao *et al.*[32] in the synthesis of mesoporous LP-FDU-12 with ultra-large pores using TMB as swelling agent. It has been reported that the associate number of micelles reduces when it approaches a critical micelle temperature (CMT) and that the copolymer molecules are less tightly aggregated in one micelle,[33,34] which benefits the penetration of hydrophobic molecules into hydrophobic cores. With the same hydrophobic property as that of TMB, the presence of $Fe(CO)_5$ simultaneously lowers the CMT of block copolymers F127. Thus, we adopted a relatively low temperature strategy at about 18 °C, which has proved to be very successful in the synthesis of the core/shell MI@CP composite. The thermogravimetric analysis result (TGA) of the as-synthesized $Fe(CO)_5$/SBA-16 shown in Fig. 6 indicates the amount of surfactant F127 assembled inside the pores was around 33 wt %. Thus, it is the surfactant F127 and $Fe(CO)_5$ precursor that penetrated into the micelle core during the assembly process.

The effects of the $Fe(CO)_5$ concentration on the surface area and pore volume of the resultant composite were also examined at the molar ratios of $Fe(CO)_5$ to TEOS = 0.37, 0.74 to 1.24. The structural parameters along with the pure SBA-16 calcined under an Ar atmosphere as a comparison are summarized in Table 1. With the increase of the molar ratio from 0 to 0.37, the surface area of the calcined sample increases from 174 to 200 $m^2\ g^{-1}$. The further increase of the molar ratio to 1.24 decreases the surface area to 47 $m^2\ g^{-1}$ and the pore volume decrease from 0.13 to 0.05 $cm^3\ g^{-1}$, attributing to the occupation of iron oxide inside the pores. The observed pore sizes were 3.9 nm and 3.5 nm for the molar ratios of 0.74 and 0.37 respectively, illustrating the swelling properties of the hydrophobic $Fe(CO)_5$ inside the pores is similar to that of TMB. With the increase of the molar ratio to 1.24, the specific surface area of the resultant materials is only 0.07 $m^2\ g^{-1}$ with a pore volume of 0.001 $cm^3\ g^{-1}$ after the removal of the silica, due to the collapse of the pores. Furthermore, sharp crystal peaks were observed in the wide-angle XRD patterns (see ESI†, Fig. S3), attributing to the decomposition of the $Fe(CO)_5$ during the hydrothermal process at 80 °C because not all of the $Fe(CO)_5$ molecules were involved in swelling the F127 molecules and some still remained in the bulk solution and tended to pyrolyse at high temperatures.[35] After considering both the magnetic properties and surface area, we chose the molar ratio of 0.74 as the most promising concentration.

Table 1 Textural parameters of the samples

Sample	Surface area [$m^2\ g^{-1}$]	Pore size [nm]	Pore volume [$cm^3\ g^{-1}$]
no $Fe(CO)_5$ calcined in Ar (pure SBA-16)	175	3.7	0.09
molar ratio $Fe(CO)_5$/TEOS = 0.37, calcined in Ar with silica in	200	3.5	0.13
MI@CP/SBA-16, calcined in Ar with silica in[a]	47	3.9	0.05
core/shell MI@CP, calcined in Ar with silica removal[a]	98	3.8/10.	0.21
calcined in air, with silica removal[a]	2.1	8	0.006
molar ratio $Fe(CO)_5$/TEOS = 1.24, calcined in Ar with silica removal	0.073	–	0.001

[a] The molar ratio of $Fe(CO)_5$/TEOS = 0.74.

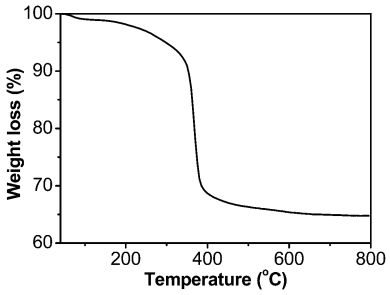

Fig. 6 TGA curve of the as-prepared $Fe(CO)_6$/SBA-16 heated up to 800 °C in air.

The adsorption of the dye methylene blue (MB) from aqueous solutions using the core/shell MI@CP composite as an adsorbent was investigated. After the addition of the core/shell MI@CP composite to the solution for less than one minute, the color of the solution changed from blue to colorless (Fig. 7a). This indicates that the MB dye was strongly adsorbed by the core/shell MI@CP, which demonstrated an excellent adsorption capacity of 70 mg g^{-1}. The loaded dye was separated by placing a conventional laboratory magnet near the glass bottle. Shown in Fig. 7a, the black particles were enriched and the dispersion became clear. The clear solution could be either decanted off or removed by pipette. This simple experiment demonstrates that the core/shell MI@CP composite is magnetic and can potentially be used as an easily recoverable adsorbent to remove dyes and other molecules in liquid-phase processes.

To study the magnetic properties of the materials in more detail, the magnetization measurements were performed at 290 K by a vibrating sample magnetometer (USM, ToeiVSM-5, USA) at room temperature and the results are given in Fig. 7b. From the plot of magnetization (M) and magnetic field (H) and its

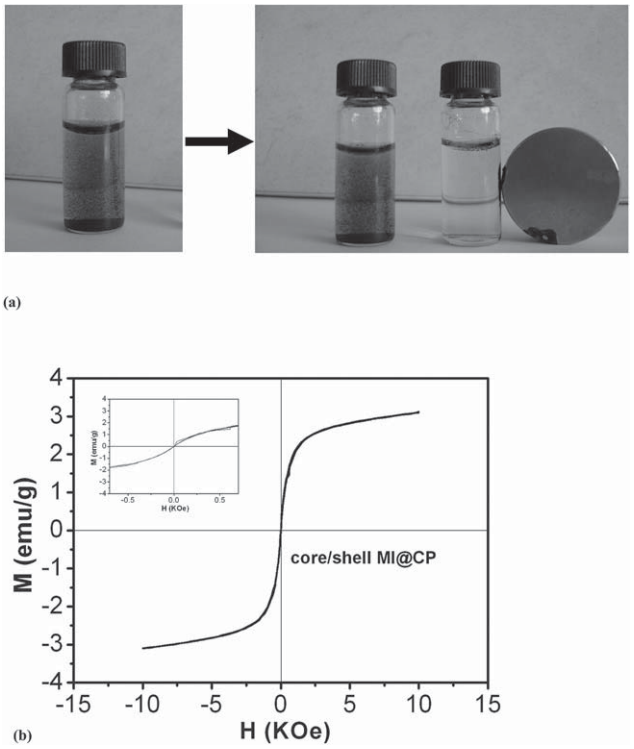

Fig. 7 (a) Methylene blue aqueous solution before, and after core/shell magnetic materials adsorption and separation of core/shell MI@CP composite from solution by a magnet, (b) magnetization curve and hysteresis loop analysis of the obtained core/shell MI@CP composite.

enlargement near the origin, it can be seen that the MI@CP composite displayed a saturation magnetization (M_s) of 3 emu g^{-1} without observable hysteresis. This suggests that the iron oxide nanoparticles were in a super-paramagnetic state. These magnetic particles can be potentially used as an adsorbent for a wide range of contaminants in water and can subsequently be removed from the solution by a simple magnetic procedure.

Conclusions

In summary, we have developed a self-templating method for the assembly of unique core/cell super-paramagnetic iron oxide/carbon porous materials, in which the magnetic nanoparticles, enveloped by a carbon layer form hybrid core/shell materials. The porous nanohybrid structures were realized through an *in situ* assembly of $Fe(CO)_5$ inside the pores of SBA-16 during a sol-gel process, and subsequent *in situ* pyrolysis to form magnetic nanoparticles inside the carbon shells. The obtained system has a high surface area (98 cm^2 g^{-1}) and large pore volume (0.21 m^3 g^{-1}), which shows its great potential in applications, such as drug delivery systems, adsorbents, or catalysis. The resultant core/shell composite has two novel properties: the porous networks make nanoparticles very accessible and the nature of the nanoparticles can be modulated by chemical specificity. It would be expected that materials with adjustable functionality by selecting different precursors and controlled architectural features by tuning structure-directing agents can be synthesized by using the method we have developed here.

Acknowledgements

The authors gratefully acknowledge the financial support of this research by the National Science Foundation of China (No. 50772067), Shanghai Science and Technology Committee(Nos.06PJ14063, 07DJ14001), and Sino-French Project of MOST of China (No.2009DFA52410). We also thank SJTU Instrument Analysis Center for the measurements.

References

1 G. M. Whitesides, *Nat. Biotechnol.*, 2003, **21**, 1161.
2 C. C. Berry, *J. Mater. Chem.*, 2005, **15**, 543.
3 A. K. Gupta and M. Gupta, *Biomaterials*, 2005, **26**, 3995.
4 S. Mornet, S. Vasseur, F. Grasset and E. Duguet, *J. Mater. Chem.*, 2004, **14**, 2161.
5 Z. Li, L. Wei, M. Y. Gao and H. Lei, *Adv. Mater.*, 2005, **17**, 1001.
6 P. A. Dresco, V. S. Zaitsev, R. J. Gambino and B. Chu, *Langmuir*, 1999, **15**, 1945.
7 X. W. Teng and H. Yang, *J. Am. Chem. Soc.*, 2003, **125**, 14559.
8 S. H. Sun, *Adv. Mater.*, 2006, **18**, 393.
9 E. V. Shevchenko, D. V. Talapin, N. A. Kotov, S. O'Brien and C. B. Murray, *Nature*, 2006, **439**, 55.
10 V. P. Torchilin, *Eur. J. Pharm. Sci.*, 2000, **11**, S81.
11 P. Tartaj, M. D. Morales, S. Veintemillas-Verdaguer, T. Gonzalez-Carreno and C. J. Serna, *J. Phys. D: Appl. Phys.*, 2003, **36**, R182.
12 Y. Lee, J. Lee, C. J. Bae, J. G. Park, H. J. Noh, J. H. Park and T. Hyeon, *Adv. Funct. Mater.*, 2005, **15**, 503.
13 J. Kim, J. E. Lee, J. Lee, Y. Jang, S. W. Kim, K. An, H. H. Yu and T. Hyeon, *Angew. Chem., Int. Ed.*, 2006, **45**, 4789.
14 R. Fernandez-Pacheco, M. Arruebo, C. Marquina, R. Ibarra, J. Arbiol and J. Santamaria, *Nanotechnology*, 2006, **17**, 1188.
15 V. Salgueirino-Maceira and M. A. Correa-Duarte, *J. Mater. Chem.*, 2006, **16**, 3593.
16 J. Kim, J. E. Lee, J. Lee, J. H. Yu, B. C. Kim, K. An, Y. Hwang, C. H. Shin, J. G. Park, J. Kim and T. Hyeon, *J. Am. Chem. Soc.*, 2006, **128**, 688.
17 J. Lee, D. Lee, E. Oh, J. Kim, Y. P. Kim, S. Jin, H. S. Kim, Y. Hwang, J. H. Kwak, J. G. Park, C. H. Shin, J. Kim and T. Hyeon, *Angew. Chem., Int. Ed.*, 2005, **44**, 7427.
18 M. Schwickardi, S. Olejnik, E. L. Salabas, W. Schmidt and F. Schuth, *Chem. Commun.*, 2006, 3987.
19 S. H. Joo, S. J. Choi, I. Oh, J. Kwak, Z. Liu, O. Terasaki and R. Ryoo, *Nature*, 2001, **412**, 169.
20 S. H. Liu, R. F. Lu, S. J. Huang, A. Y. Lo, S. H. Chien and S. B. Liu, *Chem. Commun.*, 2006, 3435.
21 L. C. A. Oliveira, R. V. R. A. Rios, J. D. Fabris, V. Garg, K. Sapag and R. M. Lago, *Carbon*, 2002, **40**, 2177.
22 A. H. Lu, W. Schmidt, N. Matoussevitch, H. Bonnemann, B. Spliethoff, B. Tesche, E. Bill, W. Kiefer and F. Schuth, *Angew. Chem., Int. Ed.*, 2004, **43**, 4303.
23 Z. H. Wen, J. Liu and J. H. Li, *Adv. Mater.*, 2008, **20**, 743.
24 J. E. Hampsey, Q. Y. Hu, L. Rice, J. B. Pang, Z. W. Wu and Y. F. Lu, *Chem. Commun.*, 2005, 3606.
25 R. Ryoo, S. H. Joo and S. Jun, *J. Phys. Chem. B*, 1999, **103**, 7743.
26 X. Q. Zhao, B. X. Liu, Y. Liang and Z. Q. Hu, *Appl. Phys. A: Mater. Sci. Process.*, 1997, **64**, 483.
27 M. H. I. Tamura, *Surf. Sci.*, 1984, **146**, 501.
28 S. Yu and G. M. Chow, *J. Appl. Phys.*, 2005, **98**, 114306.
29 C. Y. Liu, L. X. Li, H. H. Song and X. H. Chen, *Chem. Commun.*, 2007, 757.
30 A. H. Lu, A. Kiefer, W. Schmidt and F. Schuth, *Chem. Mater.*, 2004, **16**, 100.
31 S. M. Zhu, Z. Y. Zhou and D. Zhang, *ChemPhysChem*, 2007, **8**, 2478.
32 J. Fan, C. Z. Yu, J. Lei, Q. Zhang, T. C. Li, B. Tu, W. Z. Zhou and D. Y. Zhao, *J. Am. Chem. Soc.*, 2005, **127**, 10794.
33 C. Booth and D. Attwood, *Macromol. Rapid Commun.*, 2000, **21**, 501.
34 J. S. P. Kell Mortensen, *Macromolecules*, 1993, **26**, 805.
35 Q. H. S. Schacht, I. G. Voigt-Martin, G. D. Stucky and F. Schüth, *Science*, 1996, **273**, 768.